Physics in Medicine & Biology

PAPER

The importance of dead material within a tumour on the dynamics in response to radiotherapy

To cite this article: Thomas D Lewin *et al* 2020 *Phys. Med. Biol.* **65** 015007

View the article online for updates and enhancements.

This content was downloaded from IP address 129.67.187.61 on 14/01/2020 at 18:17

IOP Publishing Phys. Med. Biol. 65 (2020) 015007 (16pp) https://doi.org/10.1088/1361-6560/ab4c27

Physics in Medicine & Biology

IPEM Institute of Physics and Engineering in Medicine

CrossMark

RECEIVED
10 May 2019

REVISED
24 September 2019

ACCEPTED FOR PUBLICATION
8 October 2019

PUBLISHED
10 January 2020

PAPER

The importance of dead material within a tumour on the dynamics in response to radiotherapy

Thomas D Lewin[1,4], **Helen M Byrne**[1], **Philip K Maini**[1], **Jimmy J Caudell**[2], **Eduardo G Moros**[2] and **Heiko Enderling**[2,3]

[1] Wolfson Centre for Mathematical Biology, Mathematical Institute, University of Oxford, Oxford, United Kingdom
[2] Radiation Oncology, H. Lee Moffitt Cancer Center & Research Institute, Tampa, FL, United States of America
[3] Integrated Mathematical Oncology, H. Lee Moffitt Cancer Center & Research Institute, Tampa, FL, United States of America
[4] Author to whom correspondence should be addressed.

E-mail: tomlewin@hotmail.co.uk

Keywords: fractionated radiotherapy, cell death, multiphase mixtures, moving boundaries, tumour growth

Abstract

In vivo tumours are highly heterogeneous, often comprising regions of hypoxia and necrosis. Radiotherapy significantly alters the intratumoural composition. Moreover, radiation-induced cell death may occur via a number of different mechanisms that act over different timescales. Dead material may therefore occupy a significant portion of the tumour volume for some time after irradiation and may affect the subsequent tumour dynamics.

We present a three phase tumour growth model that accounts for the effects of radiotherapy and use it to investigate how dead material within the tumour may affect the spatio-temporal tumour response dynamics. We use numerical simulation of the model equations to characterise qualitatively different tumour volume dynamics in response to fractionated radiotherapy. We demonstrate examples, and associated parameter values, for which the properties of the dead material significantly alter the observed tumour volume dynamics throughout treatment. These simulations suggest that for some cases it may not be possible to accurately predict radiotherapy response from pre-treatment, gross tumour volume measurements without consideration of the dead material within the tumour.

Introduction

Radiotherapy is the most common cancer therapy modality, with almost half of all cancer patients receiving radiation as part of their treatment (Fowler 2006). Radiation is typically delivered to the tumour as a series of small doses, or fractions, administered over a period of several days or weeks (Ahmed *et al* 2014). While there are numerous aspects of an *in vivo* tumour biology which may influence treatment response, tumour location and stage remain the primary factors in selecting a treatment protocol (Caudell *et al* 2017).

Mathematical modelling of radiotherapy may be used to provide a better understanding of the factors which are important in determining tumour response dynamics. There are a number of approaches that may be taken to model radiotherapy response, including compartmental ordinary differential equation (ODE) models (Sachs *et al* 2001, Chvetsov *et al* 2009, Wang and Feng 2013, Chvetsov 2013, Chvetsov *et al* 2014, Prokopiou *et al* 2015, Tariq *et al* 2016), continuum partial differential equation (PDE) models (Rockne *et al* 2009, 2010, Rockne *et al* 2015, Lewin *et al* 2018), computational agent-based models (Richard *et al* 2007, Powathil *et al* 2013, 2016, Alfonso *et al* 2014) and probabilistic approaches (Zaider and Minerbo 2000, Hanin 2004, O'Rourke *et al* 2009, Zaider and Hanin 2011, Gong *et al* 2013, Bobadilla *et al* 2018). The simplest formulations view the tumour volume as a single, homogeneous compartment (Wheldon *et al* 1977, Sachs *et al* 2001, McAneney and O'Rourke 2007, Prokopiou *et al* 2015, Poleszczuk *et al* 2018) and are often targeted towards clinical application due to the limited data typically available for model calibration (Wang *et al* 2009, Stevens *et al* 2010, Sharma *et al* 2016).

The linear-quadratic (LQ) model, along with its extensions, is typically used to describe dose-dependent radiation-induced cell death (Joiner 2009). This model was initially proposed as an empirical formula derived from *in vitro* clonogenic survival assays (Joiner 2009). As such, the LQ model is most suited to describing the long-term, dose-dependent survival fraction post-irradiation, but may (inadequately) simulate the dynamics

© 2020 Institute of Physics and Engineering in Medicine

of radiation-induced cell death during fractionated radiotherapy as an instantaneous loss of material from the tumour volume (Wheldon *et al* 1977, Sachs *et al* 2001, McAneney and O'Rourke 2007, Prokopiou *et al* 2015, Poleszczuk *et al* 2018).

Upon absorption, radiation causes lesions within the cells' DNA (Joiner *et al* 2009). The damage may be fatal, with cell death occurring via one of several different mechanisms over potentially different timescales (Endlich *et al* 2000, Eriksson and Stigbrand 2010). As such, cells that are fated to die may occupy volume within the tumour for some time after irradiation and may subsequently affect the response dynamics. We may thus anticipate that the dead material within the tumour may have a significant influence on tumour volume dynamics in response to radiotherapy.

In this paper we incorporate the effects of radiotherapy into a multiphase model for tumour growth (Lewin *et al* 2019) to investigate the role of dead material on treatment response dynamics. Multiphase models which represent the microenvironment as a mixture of two or more constituent phases may be used to investigate interactions between the different components of a growing tissue (e.g. cancer cells, extracellular fluid, immune cells, vasculature and healthy cells). A range of models of this type have been proposed to study different aspects of tumour growth (Ward and King 1999, Landman and Please 2001, Breward *et al* 2002, Byrne *et al* 2003, Hubbard and Byrne 2013, Boemo and Byrne 2019, Lewin *et al* 2019). This framework provides a natural setting to investigate the influence of non-viable, dying cells and cellular debris on the spatio-temporal tumour dynamics in the context of radiotherapy response. Radiation-induced cell death may be incorporated as a mass transfer between the phases in the mixture, thus altering the internal tumour composition without instantaneous volume loss. The effect of radiotherapy on the tumour volume may then be realised as a redistribution of material within the tumour post-irradiation. Our previous work showed that the properties of the dead material may significantly affect the tumour growth dynamics (Lewin *et al* 2019). We thus anticipate that, given the changes to the internal tumour composition induced by radiotherapy, the dead material within the tumour may also have a similar impact on the treatment response dynamics.

Materials and methods

Multiphase tumour growth model

We consider a three phase tumour growth model, focussing on the influence of the dead material within the tumour on the overall tumour growth dynamics. The model treats the tumour micro-environment as a continuum, multiphase mixture, comprising three constituent phases: (i) tumour cells, (ii) dying cells and cellular debris, and (iii) extracellular fluid. The second phase is assumed to comprise all of the non-viable cellular material and cellular debris within the tumour, irrespective of cell death mechanism or stage of decay. As such, this phase represents an 'averaged' description of this component of the tumour environment across all of these modes of cell death and is a transitional phase between the viable tumour population and the extracellular fluid. We hereafter refer to this phase as 'dead material'.

The spatial distribution of each phase is characterised by the volume fractions $\phi_i(\mathbf{x}, t)$ $(i = 1, 2, 3)$ for the tumour cell, dead material and extracellular fluid phases, respectively, at spatial point $\mathbf{x}$ and time t. The phase velocities $\mathbf{v_i}(\mathbf{x}, t)$ describe the movement of each phase, and are associated with the phase pressures, $p_i(\mathbf{x}, t)$, and the stress tensors, $\underline{\boldsymbol{\sigma}}_{\boldsymbol{i}}(\mathbf{x}, t)$. We model the mixture constituents as fluids, with the tumour and dead material phases treated as viscous while the extracellular fluid is taken to be inviscid. Mass and momentum balances are applied to each phase to determine how the dependent variables evolve over time. Tumour growth is assumed to be oxygen-dependent and so the system of equations is coupled to a reaction-diffusion equation for the oxygen concentration, $c(\mathbf{x}, t)$. The full system of equations is stated below, with the detailed derivation of the model equations presented in Lewin *et al* (2019).

$$\text{Mass conservation}: \quad \frac{\partial \phi_i}{\partial t} + \nabla \cdot (\mathbf{v_i}\phi_i) = S_i \tag{1}$$

$$\text{Momentum conservation}: \quad 0 = \nabla \cdot (\phi_i \underline{\boldsymbol{\sigma}}_{\boldsymbol{i}}) + \mathbf{F_i} \tag{2}$$

$$O_2 \text{ reaction–diffusion}: \quad 0 = D\nabla^2 c - \Gamma \phi_1 H_\epsilon(c - c_N) \tag{3}$$

$$\text{where} \quad H_\epsilon(c) = \frac{1}{2}\left(1 + \tanh\left(\frac{c}{\epsilon}\right)\right) \tag{4}$$

$$\text{No voids}: \quad \sum_i \phi_i = 1 \tag{5}$$

$$\text{Mass sources and sinks}: \quad \begin{aligned} S_1 &= \eta\phi_1\phi_3 H_\epsilon(c - c_H) - \chi\phi_1 H_\epsilon(c_N - c) - \kappa\phi_1 \\ S_2 &= \chi\phi_1 H_\epsilon(c_N - c) + \kappa\phi_1 - \lambda\phi_2, \quad S_3 = -(S_1 + S_2) \end{aligned} \tag{6}$$

$$\text{Momentum sources}: \quad \mathbf{F_i} = p_i\nabla\phi_i + \sum_{j\neq i} d_{ij}\phi_j\phi_i(\mathbf{v_j} - \mathbf{v_i}) \tag{7}$$

$$\text{Stress tensors}: \quad \begin{aligned} \underline{\boldsymbol{\sigma}}_{\boldsymbol{i}} &= -p_i\underline{\mathbf{I}} + \mu_i(\nabla\mathbf{v_i} + \nabla\mathbf{v_i}^T) + \lambda_i(\nabla\cdot\mathbf{v_i})\,\underline{\mathbf{I}} \\ \lambda_i &= -\frac{2}{3}\mu_i, \quad \mu_1 \geqslant \mu_2 = \theta_\mu\mu_1 \geqslant \mu_3 = 0 \end{aligned} \tag{8}$$

$$\text{Pressures}: \quad p_1 = p + \Sigma_\phi(\phi_1 + \theta_\Sigma\phi_2), \quad p_2 = p + \theta_p\Sigma_\phi(\phi_1 + \theta_\Sigma\phi_2), \quad p_3 = p \tag{9}$$

$$\text{where} \quad \Sigma_\phi(\phi) = \frac{\zeta(\phi - \phi_{min})^2(\phi - \phi^*)}{(1-\phi)}H(\phi - \phi_{min}).$$

Here $H(\cdot)$ is the Heaviside function and $\underline{\mathbf{I}}$ denotes the identity tensor. A list of all model parameters is given in table 1.

The source and sink terms, S_i, given by equation (6) account for mass transfer between the phases and may be associated with proliferation and cell death processes. We note that proliferation is assumed to occur at a rate proportional to the product of the local volume fraction of the tumour cell phase, ϕ_1, and the extracellular fluid, ϕ_3, since the material and nutrients required for proliferation are assumed to be derived from the extracellular fluid phase.

Of particular note is the parameter vector $\boldsymbol{\theta} = (\theta_\mu, \theta_p, \theta_\Sigma)$ which describes the material properties of the necrotic phase relative to the tumour cell phase, and takes values in $[0,1]^3$. Since $\boldsymbol{\theta} \in [0,1]^3$, we may consider the dead material phase to be intermediate between the tumour cells and extracellular fluid phases. We note that $\boldsymbol{\theta} = (1,1,1)$ describes a two phase sub-case of the full model in which the dead material is essentially a compartment of the cellular phase and has the same mechanical properties as the tumour cells. Conversely, the limit $\boldsymbol{\theta} = (0,0,0)$ gives a sub-case in which the dead material has the same properties as the inviscid extracellular fluid.

The parameter θ_μ specifies the viscosity of the dead material relative to the cell phase (equation (8)). The tumour cell and dead material phase pressures contain an additional pressure, $\Sigma_\phi(\phi)$, (defined in equation (9)) which pertains to cell-sensing. The parameters ϕ^* and ϕ_{min} prescribe the thresholds for the cell-sensing effects described by the function Σ_ϕ. More specifically, when cells are sparsely distributed, adhesion forces bring the cells closer together, while in densely-packed regions the cells act to relieve stress by exerting a repulsive force on neighbouring cells (Cheng *et al* 2017). As such, when $\phi > \phi^*$, $\Sigma_\phi(\phi) > 0$ which corresponds to a repulsive cell pressure, whilst when $\phi_{min} < \phi < \phi^*$, $\Sigma_\phi < 0$ which corresponds to regions of cellular adhesion or attraction. A schematic of the function $\Sigma_\phi(\phi)$ is shown in figure 1. The parameters θ_p and θ_Σ thus describe the relative cell-sensing function of the dead material in comparison to the tumour cell phase, with Σ_ϕ evaluated locally at $(\phi_1 + \theta_\Sigma\phi_2)$.

Incorporating radiotherapy effects

Radiotherapy effects are modelled as an instantaneous mass transfer between the tumour cell and dead material phases at the time of delivery, t_j, and included in the mass source terms, S_i, as follows:

$$S_1 = \eta\phi_1\phi_3 H_\epsilon(c - c_H) - \chi\phi_1 H_\epsilon(c_N - c) - \kappa\phi_1 - \sum_j \nu(c)\phi_1\delta(t - t_j), \tag{10}$$

$$S_2 = \chi\phi_1 H_\epsilon(c_N - c) + \kappa\phi_1 - \lambda\phi_2 + \sum_j \nu(c)\phi_1\delta(t - t_j), \tag{11}$$

$$S_3 = -S_1 - S_2. \tag{12}$$

Here, $\nu(c)$ encompasses the dependence of radiation-induced cell death on the local oxygen concentration, c, and is related to the dose-dependent cell survival fraction, $SF(d)$, by $\nu = 1 - SF(d)$. In this paper we assume radiation is delivered with a uniform spatial dose distribution.

While still modelled as an instantaneous effect, the way in which radiotherapy is incorporated into this model is markedly different from the discontinuities in tumour volume introduced in other models (Wheldon *et al* 1977, Sachs *et al* 2001, McAneney and O'Rourke 2007, Prokopiou *et al* 2015, Poleszczuk *et al* 2018). In particular, here radiation results in an immediate change in tumour composition without changing the tumour radius. The effect of the radiotherapy on the total tumour volume is then driven by the resulting dynamics of the new internal distribution of the tumour constituents.

Table 1. Table of multiphase model parameters appearing in equations (1)–(9).

Symbol	Parameter
Γ	O_2 consumption rate
D	O_2 diffusion coefficient
c_∞	Normoxic O_2 concentration at exterior boundary
c_H	Tumour hypoxia threshold
c_N	Tumour necrosis threshold
ϵ	Heaviside smoothing parameter
η	Proliferation rate
κ	Apoptosis rate
χ	Necrosis rate
λ	Dead material decay rate
d_{ij}	Drag coefficient of phase j on phase i
μ_i	Viscosity of phase i
θ_μ	Relative viscosity of dead and tumour phases
θ_p	Relative 'cell-sensing' ability of dead phase
θ_Σ	Relative influence of dead phase on cell-sensing
ζ	Cell-sensing strength
ϕ^*	'Natural' cell volume fraction
ϕ_{min}	Minimum cell-sensing volume fraction

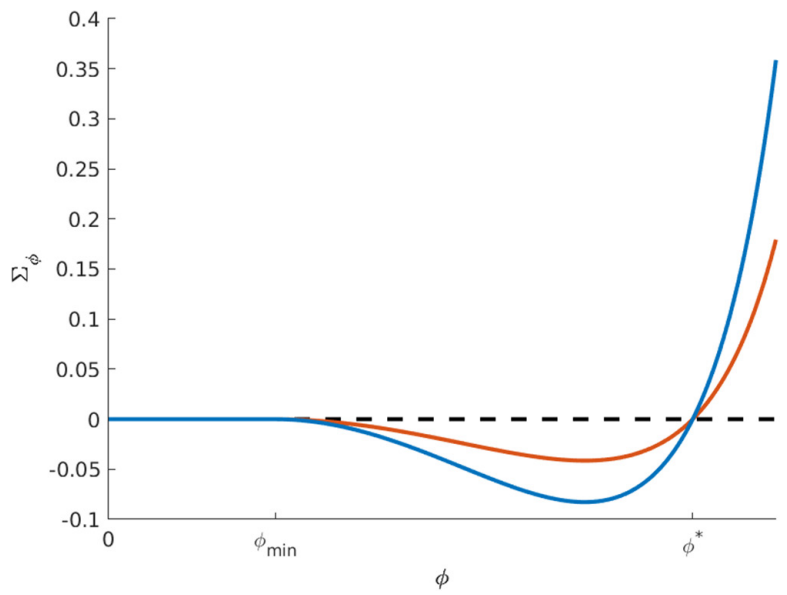

Figure 1. Illustrative sketch showing the dependence of the cell-sensing pressure $\Sigma_\phi(\phi)$ on the cell volume fraction ϕ (defined by equation (9)). We note that there is no interaction between cells if they are too sparsely seeded ($\Sigma_\phi = 0$ if $\phi \leqslant \phi_{min}$). For intermediate volume fractions the cells tend to aggregate ($\Sigma_\phi < 0$ for $\phi \in (\phi_{min}, \phi^*)$), whereas at high volume fractions the cells repel each other ($\Sigma_\phi > 0$ for $\phi \in (\phi^*, 1)$). The blue curve shows the cell sensing pressure of the tumour cell phase, while the red curve represents the corresponding pressure in the dead material phase, $\theta_p \Sigma_\phi$, for $\theta_p \in (0, 1)$.

The linear-quadratic (LQ) model is typically used to describe the dose-dependent survival fraction, $SF(d)$, of tumour cells after irradiation (Joiner and van der Kogel 2009). The standard LQ model is given by

$$SF(d) = e^{-\alpha d - \beta d^2}, \tag{13}$$

where α (Gy^{-}1) and β (Gy^{-}2) are intrinsic radiosensitivity parameters for the tissue. The response characteristics of the tumour are typically characterised by the ratio α/β (Gy) (Joiner 2009).

Various local oxygen concentrations within a tumour yield spatially heterogeneous radiosensitivities. Hypoxic tumour regions respond poorly to irradiation compared with well-oxygenated conditions. The oxygen enhancement ratio (OER; OER$\approx$ 3) is established as the conventional extension to the LQ model to account for hypoxia (Alper and Howard-Flanders 1956, Carlson *et al* 2006, Horsman *et al* 2009). This yields a step function for radiaiton sensitivity at the hypoxia threshold, c_H, given by

$$SF(d,c) = \begin{cases} \exp(-\alpha d - \beta d^2) & c \geqslant c_H \\ \exp\left(-\frac{\alpha}{OER} d - \frac{\beta}{OER^2} d^2\right) & c < c_H. \end{cases} \tag{14}$$

Reduced model equations

When closed with appropriate boundary and initial conditions, equations (1)–(5) and (7)–(14) govern the spatial and temporal dynamics of tumour growth and response to radiotherapy in three dimensions. For simplicity, we evaluate the model in a symmetrical 1D Cartesian geometry, where $x = 0$ and $x = R(t)$ denote the centre of the tumour and the (dynamic) position of the tumour boundary, respectively. As previously described, the resulting system of equations may be reduced to eliminate the fluid phase volume fraction, ϕ_3, velocity, v_3, and global pressure, p, and then be closed by specifying initial and boundary conditions (Lewin *et al* 2019). This yields the multiphase model for radiotherapy response:

Mass conservation

$$\frac{\partial \phi_1}{\partial t} + \frac{\partial}{\partial x}(\phi_1 v_1) = \eta \phi_1 (1 - \phi_1 - \phi_2) H_\epsilon(c - c_H) - \chi \phi_1 H_\epsilon(c_N - c) - \kappa \phi_1 - \sum_j \nu(c) \phi_1 \delta(t - t_j) \tag{15}$$

$$\frac{\partial \phi_2}{\partial t} + \frac{\partial}{\partial x}(\phi_2 v_2) = \chi \phi_1 H_\epsilon(c_N - c) + \kappa \phi_1 - \lambda \phi_2 + \sum_j \nu(c) \phi_1 \delta(t - t_j). \tag{16}$$

Oxygen profile

$$0 = D \frac{\partial^2 c}{\partial x^2} - \Gamma \phi_1 H_\epsilon(c - c_H). \tag{17}$$

Momentum balances

$$\begin{aligned} 0 = \frac{4}{3}\mu_1 (1 - \phi_1) \frac{\partial}{\partial x}\left(\phi_1 \frac{\partial v_1}{\partial x}\right) - \frac{4}{3}\theta_\mu \mu_1 \phi_1 \frac{\partial}{\partial x}\left(\phi_2 \frac{\partial v_2}{\partial x}\right) + d_{12}\phi_1\phi_2(v_2 - v_1) \\ - d_{13}\phi_1(\phi_2 v_2 + (1 - \phi_2) v_1) - \phi_1(1 - \phi_1)\frac{\partial \Sigma_\phi}{\partial x} + \theta_p \phi_1 \phi_2 \frac{\partial \Sigma_\phi}{\partial x} \end{aligned} \tag{18}$$

$$\begin{aligned} 0 = -\frac{4}{3}\mu_1 \phi_2 \frac{\partial}{\partial x}\left(\phi_1 \frac{\partial v_1}{\partial x}\right) + \frac{4}{3}\theta_\mu \mu_1 (1 - \phi_2) \frac{\partial}{\partial x}\left(\phi_2 \frac{\partial v_2}{\partial x}\right) + d_{12}\phi_1\phi_2(v_1 - v_2) \\ - d_{23}\phi_2(\phi_1 v_1 + (1 - \phi_1) v_2) - \theta_p \phi_2 (1 - \phi_2)\frac{\partial \Sigma_\phi}{\partial x} + \phi_1 \phi_2 \frac{\partial \Sigma_\phi}{\partial x} \end{aligned} \tag{19}$$

$$\Sigma_\phi(\phi) = \frac{\zeta(\phi - \phi_{min})^2(\phi - \phi^*)}{(1 - \phi)} H(\phi - \phi_{min}). \tag{20}$$

Initial and boundary conditions

$$\frac{dR}{dt} = v_1|_{x=R(t)} \tag{21}$$

$$\frac{\partial c}{\partial x} = 0, \quad v_1 = v_2 = 0 \quad \text{at} \quad x = 0 \tag{22}$$

$$\phi_2^+ = 0, \quad c = c_\infty \quad \text{at} \quad x = R(t) \tag{23}$$

$$\frac{4}{3}\mu_1 \frac{\partial v_1}{\partial x} - \Sigma_\phi(\phi_1 + \theta_\Sigma \phi_2) = \frac{4}{3}\theta_\mu \mu_1 \frac{\partial v_2}{\partial x} - \theta_p \Sigma_\phi(\phi_1 + \theta_\Sigma \phi_2) = 0 \quad \text{at} \quad x = R(t) \tag{24}$$

$$\phi_1 = \tilde{\phi_1}(x), \quad \phi_2 = \tilde{\phi_2}(x), \quad R = R_0 \quad \text{at} \quad t = 0. \tag{25}$$

Table 2. Table of fixed model parameter values for all simulations.

Parameter	Value
Γ	2
c_∞	1
c_H	0.3
D	1
d_{12}	1
OER	3

Table 3. Table of parameter values used for the simulations presented in the results sections.

	Growth parameters													Radiotherapy parameters		
Case	c_N	η	χ	κ	λ	d_{13}	d_{23}	ϕ^*	ϕ_{min}	μ_1	θ_μ	θ_p	θ_Σ	t_1	α	α/β
A	0.1	1	1	0.05	0.1	0.1	3	0.8	0	1	0.5	1	1	20	0.35	10
B	0.3	1	0.5	0.02	0.75	0	1	0.8	0	1	0.1	0.5	0.5	50	0.35	10
C	0.3	1	1	0.1	0.75	0.1	2	0.7	0	5	0.5	1	0.25	50	0.5	15
D	0.2	1.5	0.3	0.1	0.5	0	2	0.7	0	3	0.25	1	1	50	0.1	5
E	0.2	0.5	2	0.02	0.1	0	2	0.6	0	2	0.5	1	0.75	10	0.1	10
F	0.2	1.5	0.3	0.02	0.75	0	1	0.8	0	2	0.5	0.5	0.75	25	0.35	10
G	0.3	0.5	0.1	0.1	0.5	0	3	0.6	0	0.5	1	0.5	1	50	0.35	15
H	0.1	1	0.3	0.1	0.25	0.1	3	0.6	0	5	0.5	0.75	0.25	50	0.35	15

Results

The parameter values used for the results presented in this paper are listed in tables 2 and 3. The values of the radiotherapy parameters are taken from ranges reported in the literature (Joiner and van der Kogel 2009), while the remaining parameter combinations are taken from the exploration of the model parameter space presented in Lewin *et al* (2019). We note that typical values for many of the model parameters are not available in the literature. As a result, we treat the parameters as dimensionless and perform a qualitative exploration of the model dynamics across the parameter space.

Response to a single radiation fraction

We first analyse tumour response to a single radiation fraction with dose $d = 2$ Gy. The step function formulation of the OER results in a jump in the tumour cell volume fraction ϕ_1 on either side of the pre-radiotherapy contour $x = R_H(t_1^-)$ due to the effects of normoxia and hypoxia on the survival fraction of the tumour population (figure 2(a)). The loss of mass from the tumour cell phase results in re-oxygenation within the tumour and, correspondingly, the hypoxia threshold ($R_H(t)$) moves towards the centre of the tumour such that $R_H(t_1^+) < R_H(t_1^-)$. However, the outer tumour radius, R, does not experience an instantaneous jump and $R(t_1^+) = R(t_1^-)$. The composition change within the tumour induces a change in the phase velocities, v_i. In particular, $v_1(R(t_1^+), t_1^+) < 0$ and thus the tumour radius decreases gradually and transiently after irradiation (figure 2(b)). Regrowth dynamics post-irradiation are affected by the redistribution of material within the tumour. The volume fractions smooth out over time as the material gradually redistributes towards pre-irradiation composition. However, redistribution of material internally affects the growth trajectory with lower velocities of the tumour boundary, $v_1(R(t), t)$ compared to similar radii before radiation (figure 2(c)).

Tumour dynamics in response to fractionated radiotherapy

Tumour volume response dynamics after fractionated radiation vary between individual patients. Semi-automated contouring of cone beam computed tomography (CBCT) images routinely obtained for patient positioning at each radiation fraction allows for measurement of gross tumour volume (GTV) (Bagher-Ebadian *et al* 2017) and indicates four qualitatively different responses. For demonstration purpose we show that these different dynamic responses can be observed in oropharyngeal cancer patients with comparable stage and size at beginning of radiotherapy (43.7 cm^3, 48.5 cm^3, 63.3 cm^3 and 48.7 cm^3, figure 3). The data shown is from a cohort of 51 oropharyngeal cancer patients comprised of 32 who were treated at Moffitt Cancer Center, Florida and 19 at MD Anderson, Texas (Lewin *et al* 2016). Each patient received the standard fractionation protocol with 2 Gy fractions administered daily Monday–Friday.

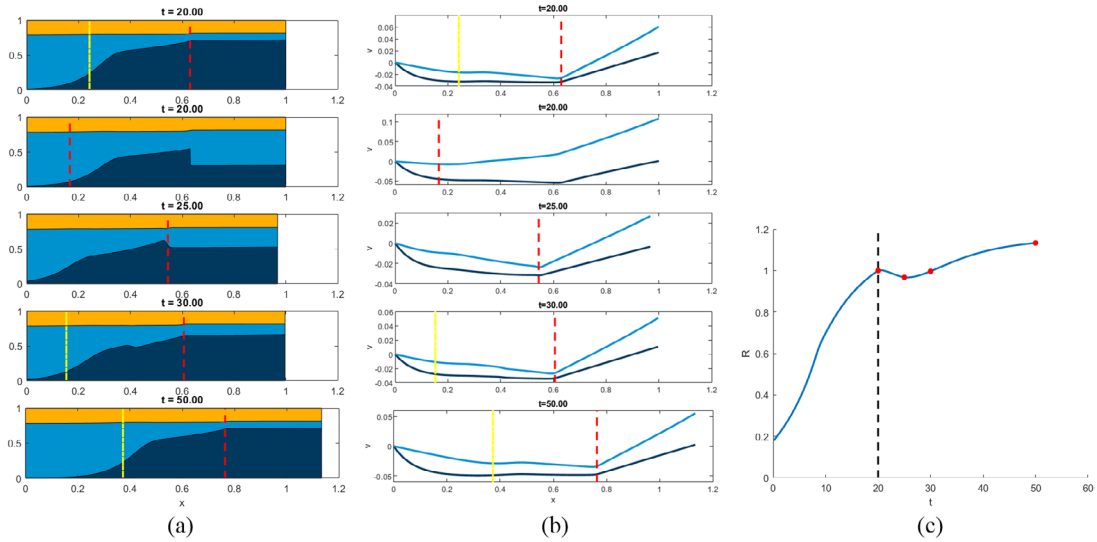

Figure 2. Representative simulation of multiphase tumour response to acute radiation with dose $d = 2$ Gy at time $t = 20$ using model parameters in table 2 and radiosensitivity parameters $\alpha = 0.35\,\mathrm{Gy}^{-1}$ and $\alpha/\beta = 10$ Gy. The remaining parameter values for this simulation are given in table 3, case A. Time series of: (a) tumour compositions, and (b) phase velocities for the simulation shown in panel (c). Individual plots show tumour composition at each time point, with the first and second time points in each series corresponding to the time steps immediately before and after irradiation at $t_1 = 20$. Tumour compositions: tumour cell volume fraction, ϕ_1 (dark blue); dead material phase, ϕ_2 (light blue); extracellular fluid volume fraction, ϕ_3 (yellow). The dashed red and yellow lines mark the positions of the contours $x = R_H$ and $x = R_N$, respectively. Phase velocities: tumour phase velocity, v_1 (dark blue); dead phase velocity, v_2 (light blue). (c) Tumour radius trajectory before and after a single fraction of radiation (2 Gy) delivered at $t_1 = 20$ (dashed black line). The solution has been normalised to the tumour radius at the time of irradiation. Red circles mark the time points of tumour composition and phase velocities plots in panels (a) and (b).

A desirable fast response is characterized by a rapid, monotonic reduction in gross tumour volume and a final tumour volume that is substantially smaller than that prior to treatment (figure 3(a)). The multiphase model simulates such a response using parameters listed in table 3, case B (figure 4(a)). By contrast, a poor response with only marginal changes in tumour volume over time is not effective in reducing the gross tumour volume (figure 3(b)). Such dynamics can be simulated with parameter combination in table 3, case C (figure 4(b)).

A third radiation response pattern is described by a decrease in tumour volume before levelling-off after which radiation has minimal effect on the measured volume (figure 3(c)). Multiphase model simulations suggest that tumour regrowth over the weekend is sufficient to counteract radiation-induced cell death in the latter stages of treatment (figure 4(c)). The tumour radius, $R(t)$, undergoes oscillations driven by the weekly fraction schedule, but once-a-week tumour volume measurements would reveal no net treatment effect. The parameter values used for this simulation are listed in table 3, case D. The step function form of the OER results in a local maximum in the tumour cell phase volume fraction, ϕ_1. At this location within the tumour $v_1 < 0$, and the volume fraction profile moves inwards. As the different cell material is redistributed the tumour composition smooths out. Tumour composition after a weekend break is almost identical to that of the previous week, indicative of the plateau in response (figure 5).

The last response dynamic is so-called 'pseudo-progression', characterised by transient increase in tumour volume during the early phase of radiotherapy, before exhibiting a delayed decrease in tumour volume (figure 3(d)). These dynamics can be simulated using $\theta_\Sigma = 0.75$ such that radiation-induced dead cell material still contributes significantly to tumour volume (figure 4(d)). At the beginning of radiotherapy, the internal tumour composition is still approximately uniform and so we may use the averaged quantities

$$\bar{\phi}_i(t) = \frac{1}{R(t)} \int_0^{R(t)} \phi_i(x,t)dx \tag{26}$$

to evaluate tumour dynamics. Figure 6 shows $\bar{\phi}_1 + \theta_\Sigma \bar{\phi}_2$ over time to evaluate cell pressures occurring within the tumour throughout the course of the treatment protocol. Quantities greater than ϕ^* correspond to positive, repulsive pressures, while those less than ϕ^* give rise to adhesive forces. Since θ_Σ is large, the value of $\bar{\phi}_1 + \theta_\Sigma \bar{\phi}_2$ does not decrease significantly upon individual radiation fractions despite the instantaneous mass transfer between the tumour cell and non-viable phases. Thus, $\bar{\phi}_1 + \theta_\Sigma \bar{\phi}_2 > \phi^*$ for the first few radiation weeks and the tumour volume continues to increase. However, the accumulated effects of radiotherapy by week 3 yield $\bar{\phi}_1 + \theta_\Sigma \bar{\phi}_2 < \phi^*$ and induce a decrease in tumour volume, which persists for the remainder of the simulated treatment. Model simulation suggest that pseudo-progression may, at least in part, be driven by a build-up of non-viable cells and dead material within the tumour, rather than an increase in the viable tumour cell population.

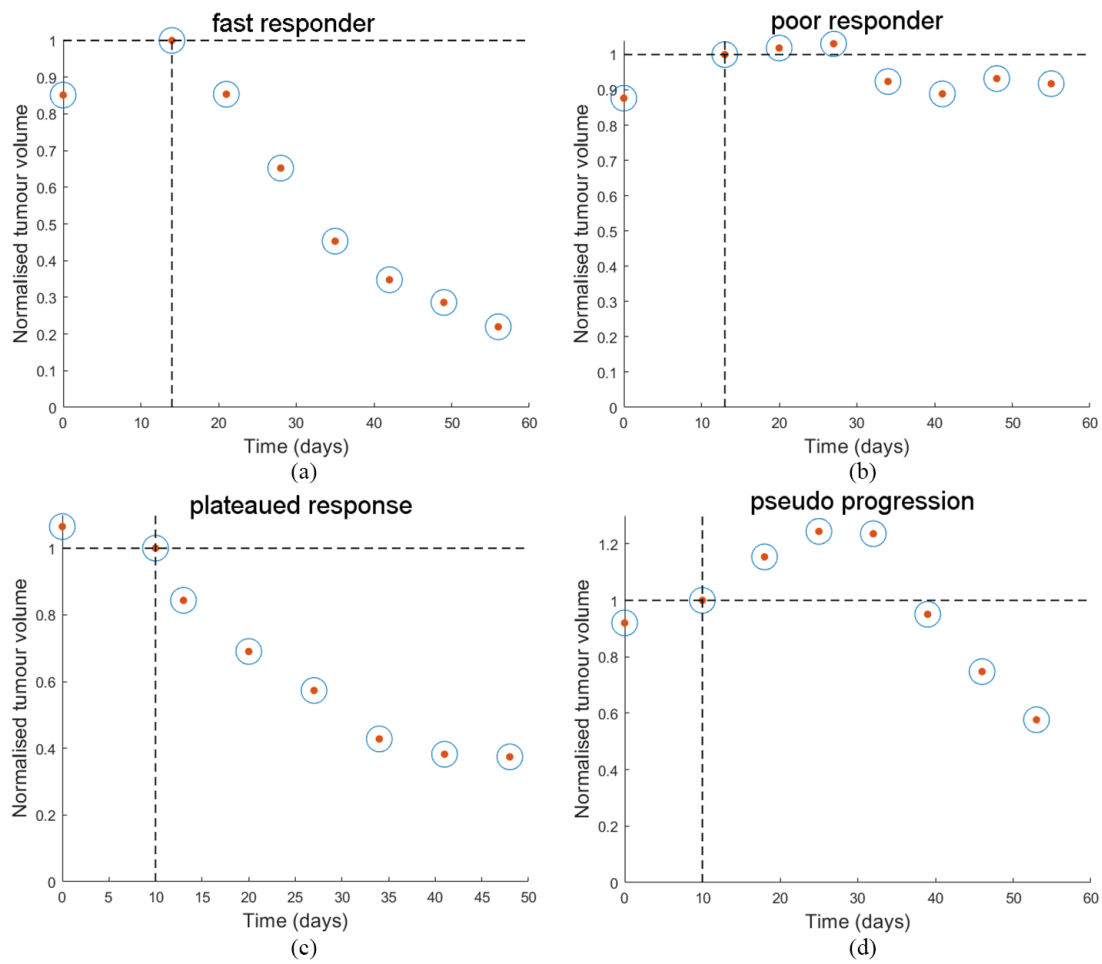

Figure 3. Representative examples of four qualitatively different radiotherapy response dynamics. The gross tumour volumes were obtained from pre-radiation treatment planning scans and weekly CBCT scans during treatment. Dashed black lines indicate start of treatment and pre-treatment tumour volume. (a) Fast responder. (b) Poor responder. (c) Response plateau. (d) Pseudo-progression.

The influence of dead material on radiotherapy response

We have previously demonstrated that, for some parameter regimes, tumour growth may be significantly affected by the physical properties of the dead material within the tumour (Lewin *et al* 2019). Here, we perform a focussed parameter sweep on the parameter subspace $(\theta_\mu, \theta_p, \theta_\Sigma) = \boldsymbol{\theta} \in [0, 1]^3$ in order to investigate the influence of the material properties of the dead phase on the tumour dynamics in response to radiotherapy. In each case all other model parameters are held fixed, including the radiosensitivity parameters. We highlight two different parameter regimes; parameters for which the properties of the dead material do not significantly affect the qualitative dynamics (left column of figure 7), and parameters for which the dynamics vary markedly across $\boldsymbol{\theta} \in [0, 1]^3$ (right column of figure 7).

In figure 7(a) we observe tumour radius trajectories which all follow similar growth dynamics while also exhibiting a similar response to radiotherapy. Each trajectory may be classified as a 'fast responder' to treatment and we note that the predicted final tumour radii are all clustered together around small values, $R < 0.3$ (see figure 7(c)). In particular the properties of the dead material phase do not appear to significantly affect the tumour dynamics either before, during or after radiotherapy, with all combinations simulated giving rise to the same qualitative response (see figure 7(e)). As such we would anticipate that a less complex model could adequately describe the observed response in this case, without necessarily taking into account the spatial distribution of the tumour composition.

By contrast, for the case presented in figure 7(b), varying the material properties results in a large degree of heterogeneity in the tumour response dynamics. The qualitative behaviours exhibited include fast response to treatment (blue), pseudo-progression (purple) and actual tumour progression throughout treatment (red). In this case the parameter sweep results in divergent trajectories with a large variation in the size of the tumour at the end of treatment (see figure 7(d)). We see that the properties of the dead material may have a significant impact on the response to treatment while holding the radiosensitivity parameters of the tumour fixed. In figure 7(f) we

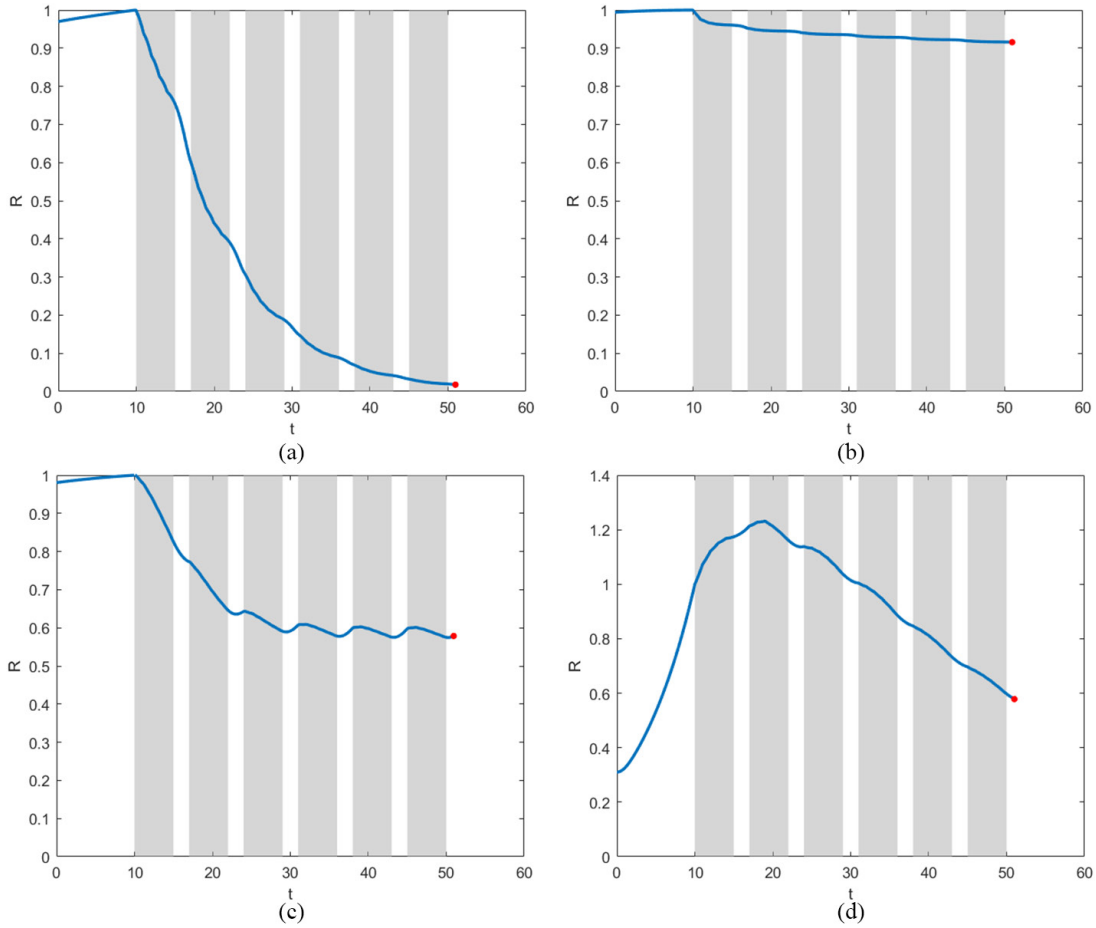

Figure 4. Simulations of equations (15)–(25) exhibiting different qualitative responses to radiotherapy with respect to the dynamics of the outer tumour radius throughout treatment. The radiotherapy protocol is represented by the grey shaded regions. The solutions have been normalised to the tumour radius at the start of treatment at time $t = 10$. The parameter values for these simulations are listed in table 3. (a) Example of a 'fast responder' to radiotherapy treatment (case B). (b) Example of a 'poor responder' to radiotherapy treatment (case C). (c) Example of a response to radiotherapy exhibiting a plateau in treatment effect (case D). (d) Example of response to radiotherapy exhibiting 'pseudo-progression' of the tumour (case E).

see that, in this parameter regime, larger values of θ_Σ result in poorer treatment responses. We further illustrate these results by analyzing the dynamics of the parameters corresponding to the two corners of the unit cube, $\boldsymbol{\theta} = (0.01, 0.01, 0.01)$ and $\boldsymbol{\theta} = (1, 1, 1)$. The model equations are singular for $\theta_\mu = 0$ so we instead choose positive values of $(\theta_\mu, \theta_p, \theta_\Sigma)$ close to 0. There is little difference in tumour composition and growth trajectories prior to treatment. Therefore, it would not be possible to distinguish between these two cases from pre-treatment radiological data even with resolution of the underlying tumour composition. However, radiation induces large perturbations to the tumour composition, and the properties of the non-viable phase may subsequently affect the redistribution of material within the tumour and therefore response dynamics (figure 8).

Tumour regrowth dynamics

Post-radiotherapy decrease in tumour volume

In the previous results section we identified a class of dynamics for which the tumour volume initially responds well to irradiation before experiencing a diminished treatment effect, or plateau, towards the end of the protocol. In this case, the regrowth of the tumour over the weekend break in the latter stages of the treatment protocol is sufficient to compensate for the volume lost due to irradiation. The tumour thus reaches a plateau in response, with no net treatment effect observed. However, in our simulations we also identify another mode of response for which the tumour volume plateaus towards the end of treatment (figure 9(a)). This response is qualitatively different to the case shown in figure 4(c). In figure 9(a) we see that the plateau in the tumour radius trajectory is such that $\frac{dR}{dt} = 0$, in contrast with the oscillations between death and regrowth driven by the on-off nature of the treatment protocol observed in figure 4(c). These dynamics are also characterised by a dip in tumour volume some time after the end of the last fraction of radiotherapy, before an increase in the tumour radius $R(t)$ and regrowth of the tumour. The parameters for the simulation shown in figure 9 are listed in table 3, case G.

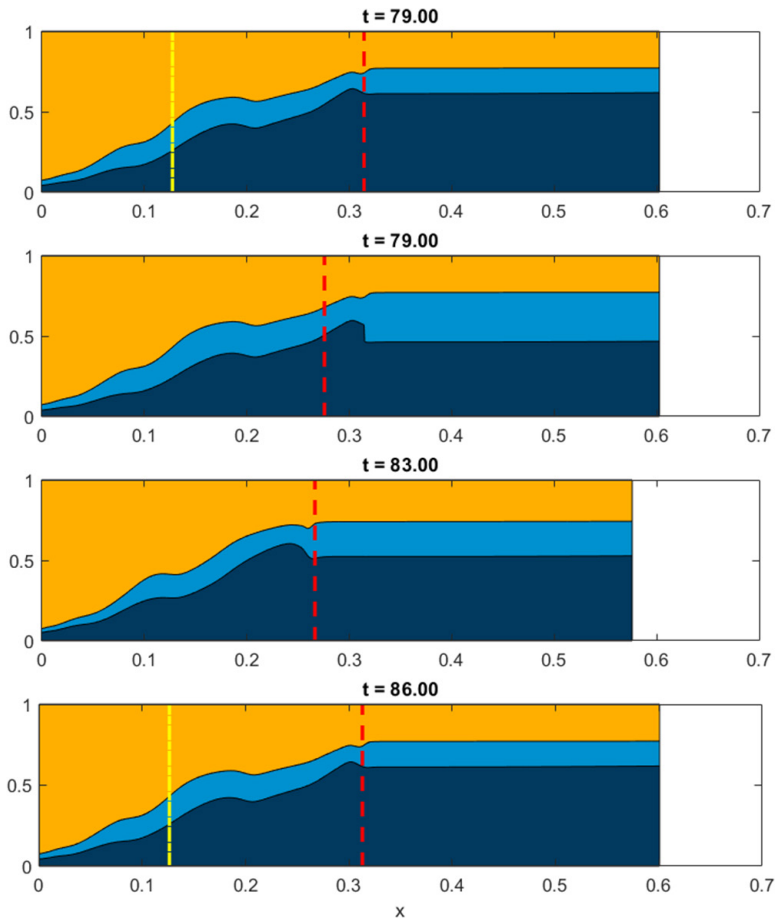

Figure 5. Time series of tumour compositions spanning a week of the fractionation protocol for the simulation presented in figure 4(c). The second time point corresponds immediately after irradiation at time $t = 79$. The volume fractions ϕ_1, ϕ_2 and ϕ_3 are represented by the dark blue, light blue and yellow regions, respectively. The dashed red and yellow lines mark the positions of the radii for the hypoxia threshold, $R_H(t)$, and necrotic threshold, $R_N(t)$, respectively. The parameter values for this simulation are given in table 3, case C.

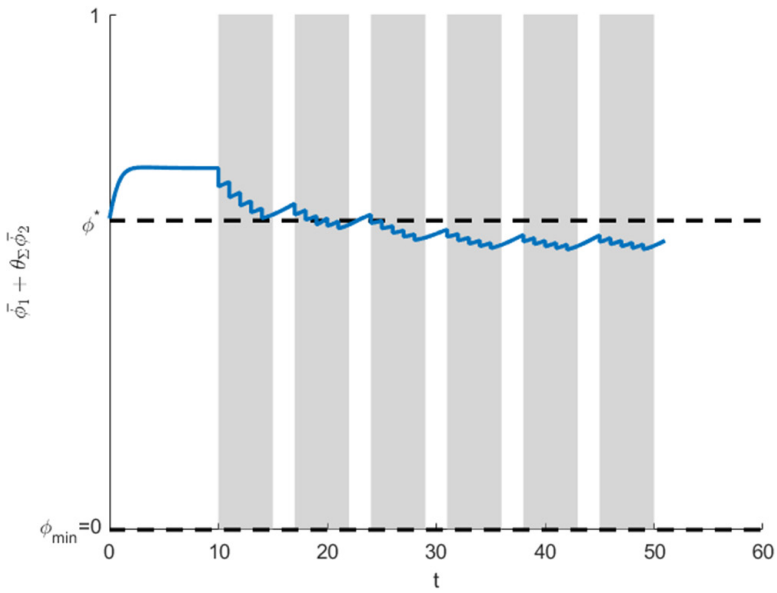

Figure 6. Plot showing $\bar{\phi}_1 + \theta_\Sigma \bar{\phi}_2$ over time for the simulation shown in figure 4(d). The quantities $\bar{\phi}_i$ represent the volume fraction of phase i averaged over the whole tumour at time t, as defined by equation (26).

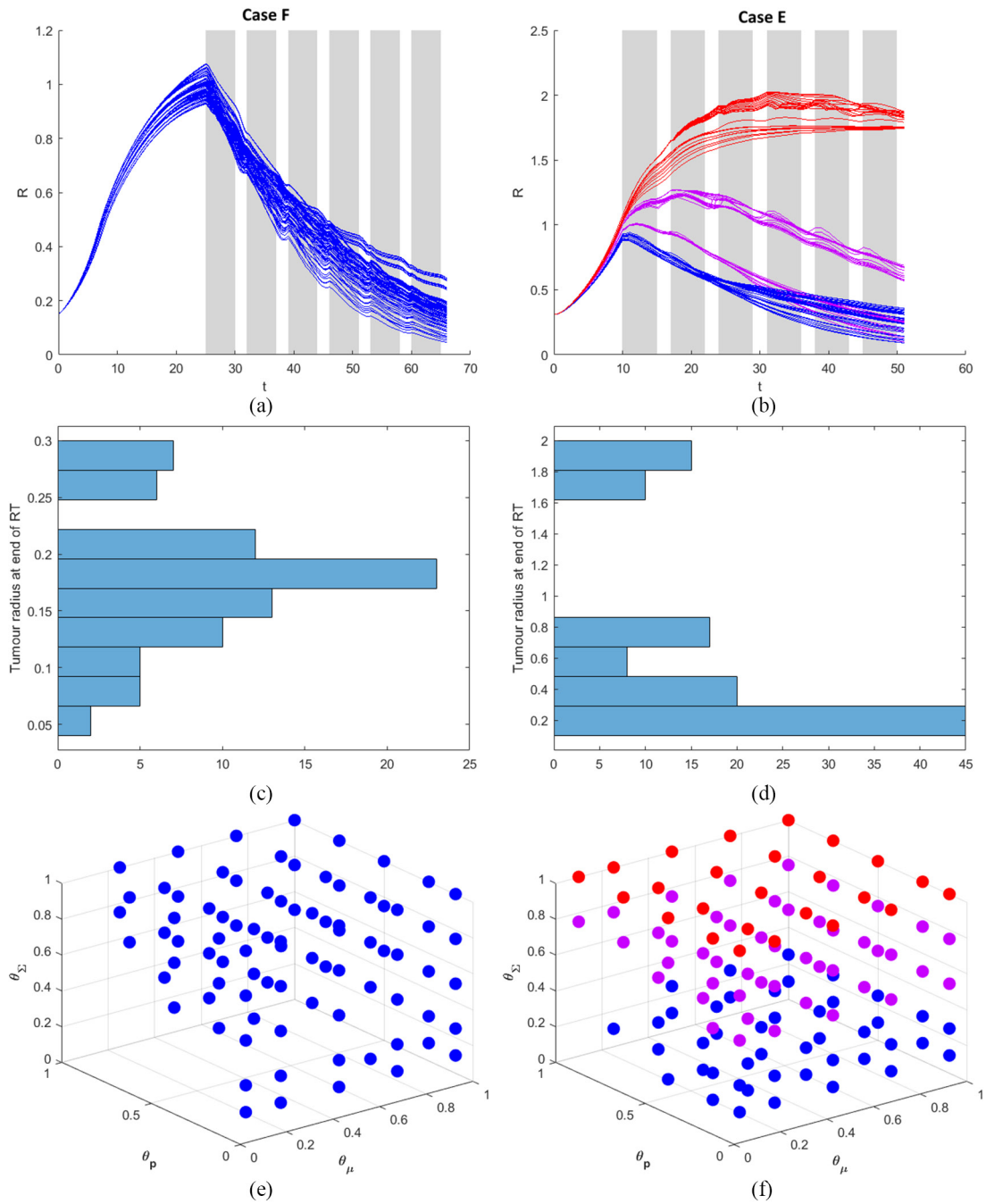

Figure 7. The results obtained by sweeping over the parameter sub-space $\boldsymbol{\theta} = (\theta_\mu, \theta_p, \theta_\Sigma) \in [0, 1]^3$ summarising the material properties of the dead phase for two different parameter regimes; one in which the dynamics remain qualitatively similar varying $\boldsymbol{\theta}$, and one for which the trajectories diverge. The parameter values for each case are given in table 3, with the parameters pertaining to the results in the left hand column given by case F, and those for the right-hand column by case E. The solutions have been normalised in each case to the radius at the start of treatment for the corresponding parameter sets given in table 3. (a) and (b) Tumour radius trajectories for each simulation in the parameter sweep. Trajectories are coloured by the qualitative response to treatment exhibited: fast responder (blue), pseudo-progression (purple) or progression (red). The radiotherapy protocol is represented by the grey shaded regions. (c) and (d) Histograms displaying the distribution of tumour radii at the end of the radiotherapy protocol for each of the parameter sweeps. (e) and (f) Scatter plot marking the qualitative response dynamics resulting from each combination of $\boldsymbol{\theta}$.

These two modes of response plateau are very different with regards to the underlying tumour composition and thus the actual efficacy of the radiotherapy, despite both simulations resulting in a diminished treatment effect while the tumour is still of significant radius. In figure 9(c) we visualise the tumour composition at 5 different time points throughout the regrowth period of the tumour after radiotherapy. We notice that at the end of treatment the tumour cell population is actually very small, contrary to what might be expected from measuring the outer tumour radius (see composition at $t = 100$). In this case, the plateau in tumour radius is not due to a lack of effect of the radiotherapy on the tumour cell population. The radiation actually kills the tumour population faster than the effects of adhesion such that $\phi_1 + \theta_\Sigma \phi_2 \leqslant \phi_{min}$. The tumour cells therefore become too

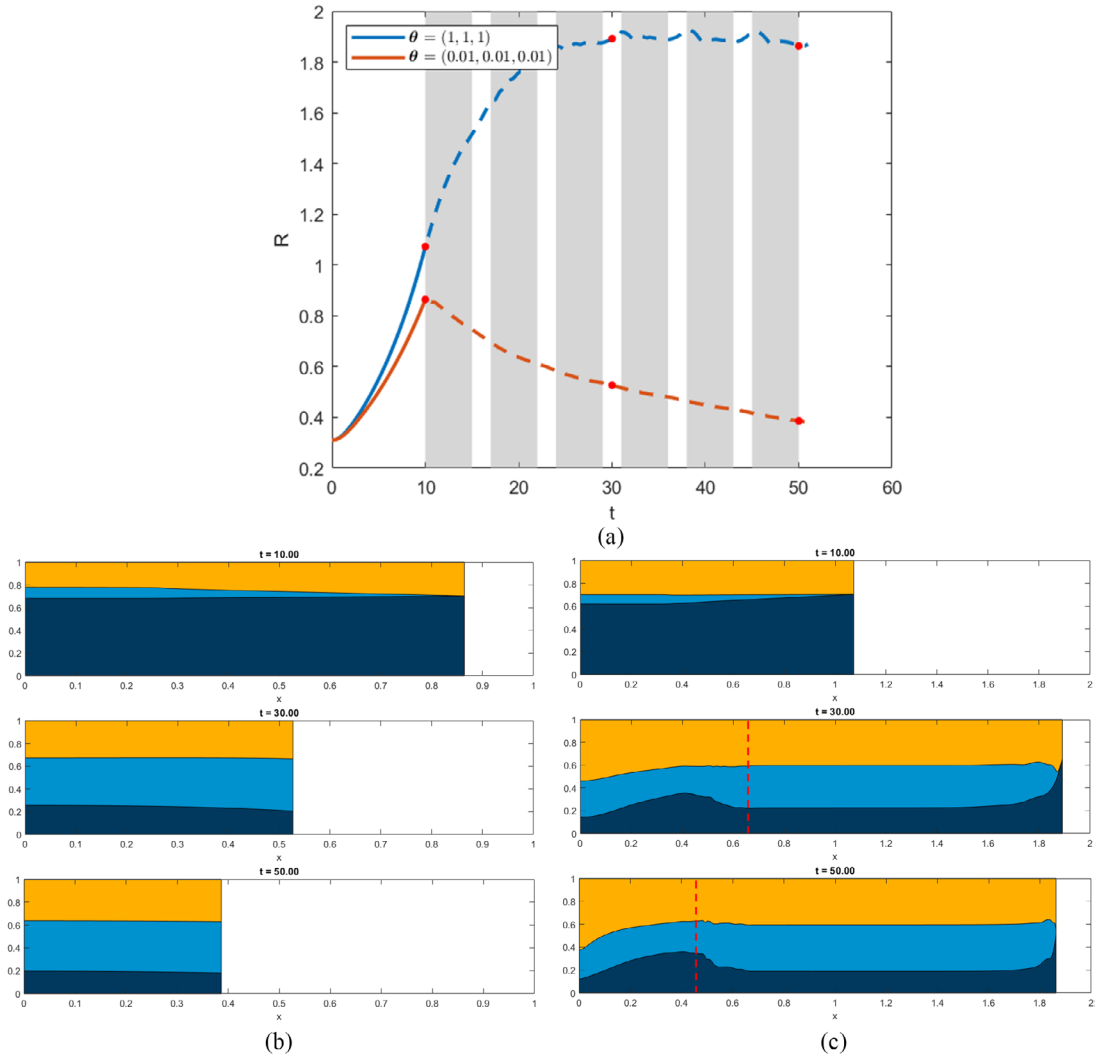

Figure 8. Two simulations of equations (15)–(25) exhibiting a large variation in response to radiotherapy, taken from the parameter sweep in figure 7(b). (a) Two tumour radius trajectories corresponding to $\boldsymbol{\theta} = (0.01, 0.01, 0.01)$ (red) and $\boldsymbol{\theta} = (1, 1, 1)$ (blue). The red points mark the time points for which we visualise the compositions in (b). (b) and (c) Tumour compositions for each simulation prior to radiotherapy at $t = 10$, during the radiotherapy protocol at $t = 30$, and at the end of treatment at $t = 50$. The simulations in (b) correspond to $\boldsymbol{\theta} = (0.01, 0.01, 0.01)$ while (c) corresponds to $\boldsymbol{\theta} = (1, 1, 1)$.

sparsely populated to interact with each other, and so the tumour radius is unable to contract further. Subsequent fractions of radiation thus kill tumour cells and reduce the volume fraction ϕ_1 locally without inducing a change in the tumour volume as measured by the outer tumour radius. The value of $\Sigma_\phi(\bar{\phi_1} + \theta_\Sigma \bar{\phi_2})$ at $t = 100$ is represented by the green dot in figure 9(b).

In a similar manner, the regrowth of the tumour cell phase after the end of the treatment protocol initially occurs locally. Once the tumour composition is such that $\Sigma_\phi(\phi_1 + \theta_\Sigma \phi_2) < 0$ the tumour cells are able to interact and cellular adhesion results in a contraction of the tumour (see time $t = 107.5$ in figure 9). While $\phi_{min} < \phi_1 + \theta_\Sigma \phi_2 < \phi^*$, the tumour radius continues to decrease and $\bar{\phi_1}$ increases due to both proliferation of the tumour cells and contraction of the tumour volume. The point at which $\bar{\phi_1} + \theta_\Sigma \bar{\phi_2} = \phi^*$ corresponds to the minimum radius in this post-radiotherapy dip such that $\frac{d^2R}{dt^2} > 0$ (see time $t = 109.5$). Thereafter, $\bar{\phi_1} + \theta_\Sigma \bar{\phi_2} > \phi^*$ and the tumour assumes a regrowth trajectory similar to that prior to treatment.

Altered regrowth dynamics

As described in the previous sections, as well as affecting the overall tumour volume, radiotherapy induces a large change in the underlying tumour composition in our multiphase mixture. In some cases, this perturbation is significant enough to completely alter the qualitative growth dynamics post-treatment when compared with the control growth trajectory in the absence of radiotherapy. The tumour radius trajectory for one such simulation is shown in figure 10 (solid blue line) along with the corresponding control growth trajectory (dashed blue line). The parameter values pertaining to this simulation are given in table 3, case H.

In this case, the original tumour growth would have given a monotonic, sigmoidal trajectory approaching a steady state solution. However, the regrowth post-radiotherapy clearly results in a travelling wave solution. The

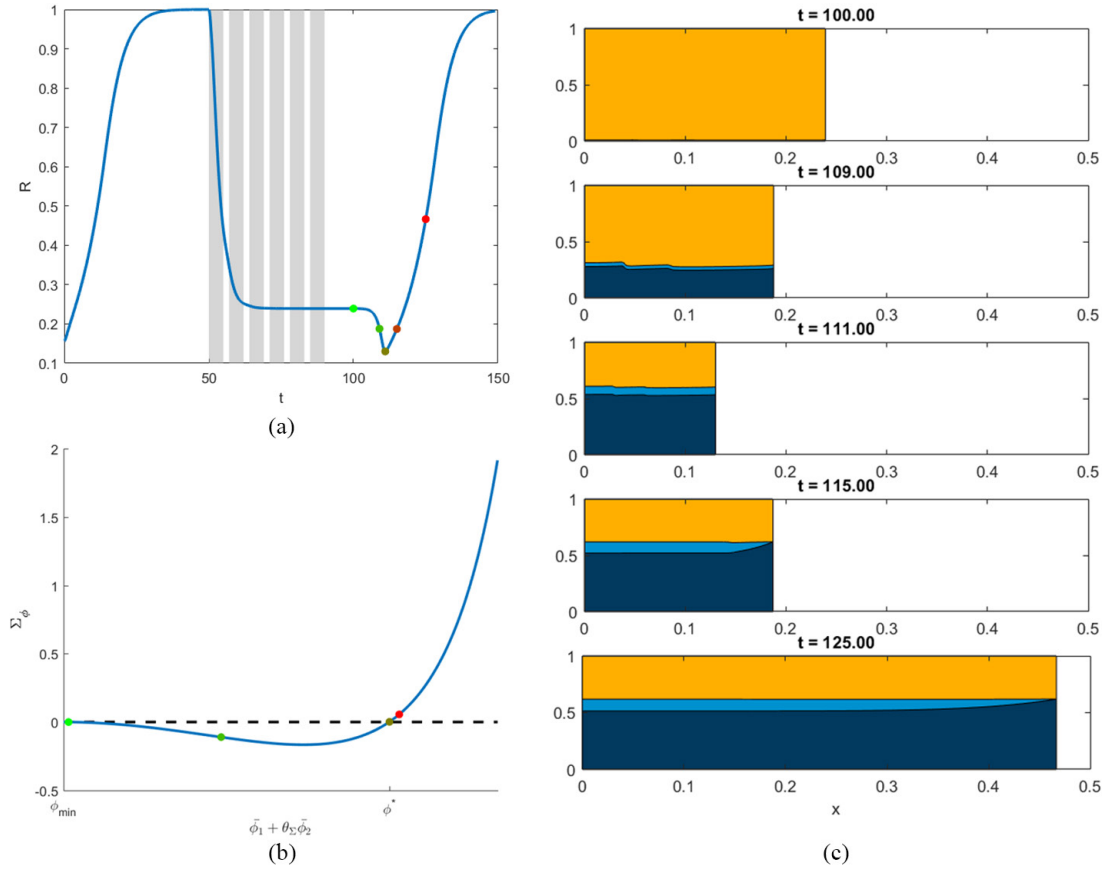

Figure 9. Simulation of equations (15)–(25) exhibiting a dip in tumour radius after the end of the radiotherapy fractionation schedule, using the parameter values in table 3, case G. The solution has been normalised to the tumour radius at the start of treatment at time $t = 50$. (a) Tumour radius trajectory (blue line) for the simulation. The dots plotted along the trajectory mark the key time points in the dynamics. (b) The cell sensing function Σ_ϕ (blue line) defined by equation (20). The points plotted mark the approximate cellular pressures within the tumour, $\Sigma_\phi(\bar{\phi}_1 + \theta_\Sigma \bar{\phi}_2)$, for the time points plotted in panel (a). (c) The corresponding tumour compositions for the time points marked on the trajectory in panel (a).

parameter regime here clearly gives rise to growth dynamics which exhibit bistability, with both steady state and travelling wave solutions possible. By significantly altering the underlying tumour composition, it is possible to change the qualitative growth dynamics of the tumour.

Discussion

Irradiation of *in vivo* tumours causes widespread cell death throughout the tumour. In particular, the dead material within the tumour may not be confined to regions of necrosis induced as a result of nutrient starvation. As such, radiotherapy induces a significant change in the intratumoural composition during the course of treatment, which differs from the pre-treatment tumour. Herein we discussed a multiphase tumour growth model to simulate radiation-induced cell death and to investigate how the redistribution of material between the tumour cell and dead material phases affects tumour volume dynamics in response to radiotherapy. We incorporated the effects of radiotherapy as an instantaneous mass transfer between the tumour cell phase and the non-viable phase. This corresponds to a redistribution of material internally within the tumour whilst avoiding the instantaneous volume loss often observed in radiotherapy response models (Enderling *et al* 2009, Rockne *et al* 2010, Prokopiou *et al* 2015, Chvetsov *et al* 2017).

We used numerical simulation of the model system to simulate radiotherapy fractionation protocols and investigate the resulting tumour response dynamics. The model exhibits a range of dynamics that are qualitatively similar to those observed in clinical data. For the class of response for which the tumour plateaus in tumour radius after an initial positive response to treatment, we observe dynamics that are very similar in nature to the results presented in our previous tumour spheroid model (Lewin *et al* 2018) whereby the weekend break allows for sufficient regrowth to overcome the effects of radiotherapy. The multiphase model presented here is also able to capture a 'pseudo-progression' response to radiotherapy. In these cases the tumour appears to continue tumour growth throughout the initial stages of treatment before a reduction in tumour volume is observed during the latter stages of the protocol. In our model, this behaviour is attributed to a build-up of dead material

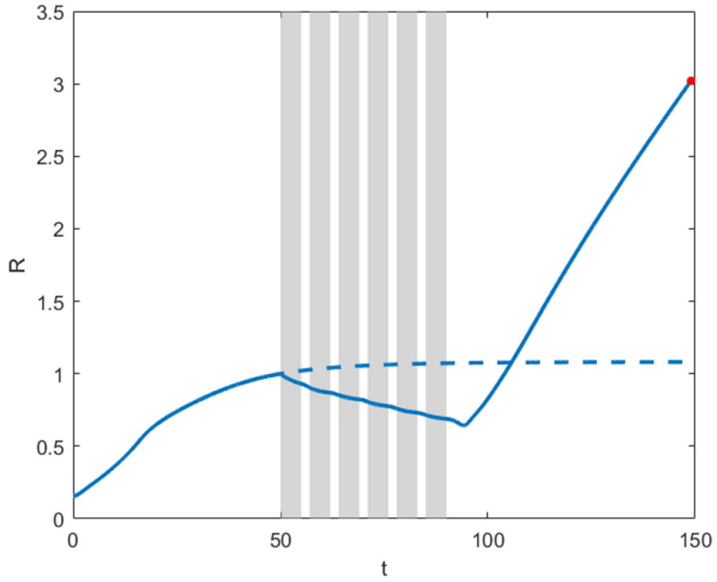

Figure 10. Tumour radius trajectory (solid blue line) for a simulation of equations (15)–(25) for which the radiotherapy alters the regrowth trajectory of the tumour. The growth trajectory in the absence of radiotherapy is shown by the dashed blue line. The solutions have been normalised to the tumour radius at the start of treatment at time $t = 50$. The parameter values for this simulation are listed in table 3, case H.

within the tumour, as opposed to an aggressive tumour population which continues to increase despite irradiation. We note that this type of response is not possible to achieve with models which treat the effects of radiotherapy as an instantaneous volume loss (Prokopiou *et al* 2015).

We characterised two different types of regrowth behaviour post-radiotherapy that differ from the growth dynamics presented in Lewin *et al* (2019). These dynamics were driven by aspects of the underlying tumour composition, highlighting the potential importance of the spatial distribution of constituents of the tumour microenvironment on the resulting dynamics. Analysis of the waiting time before the decline in tumour radius would proceed in a similar manner to that presented in (Breward *et al* 2002). Rigorous analysis of the tumour radius trajectory throughout post-treatment dynamics is likely to be tractable but is left as further work. Further investigation of the bistability is also a possible direction for future work.

The qualitative exploration of parameter space presented in this paper demonstrates the range of dynamic behaviours exhibited by our multiphase model. However, estimates of typical values for many of the model parameters are not currently available. A comprehensive exploration of clinically-relevant regions of parameter space is an important avenue for future work. The field of clinical imaging to measure tumour/normal tissue physiology (e.g. cell density, hypoxia, proliferation) is rapidly advancing (Sun *et al* 2018, Salem *et al* 2019, Rockne *et al* 2019). New techniques may soon provide spatiotemporal data with which to parametrise our model and those of others.

The local structure of the tumour vasculature is known to have a strong influence on *in vivo* tumour growth and treatment response (Bertout *et al* 2008, Hanahan and Weinberg 2000, Carmeliet and Jain 2000). Several existing models aim to investigate the effects of tumour vasculature on radiotherapy response (Ergun *et al* 2003, Ledzewicz and Schättler 2012, Scott *et al* 2016, Grogan *et al* 2016). In this paper we neglected explicit mention of the vasculature and focussed our attention on the influence of the internal tumour composition on the qualitative response to irradiation. While the full model system (equations (1)–(9)) generalises to 3D, we used numerical simulations in a simplified 1D Cartesian geometry to examine the model dynamics. Future work would include simulating the model dynamics for more complex geometries. In this setting the model could be further extended to incorporate tumour vasculature (Hubbard and Byrne 2013) to investigate the interplay between vascular density, cell death and radiotherapy. Similarly, several authors have investigated the dependence of the oxygen enhancement ratio, *OER*, on the local oxygen concentration (Carlson *et al* 2011). Simulations using a more complex functional relationship did not show significant differences and so here we favour the simplest form for incorporating the effects of hypoxia on radiotherapy response. Further investigation of these effects in more complex geometries is an area for further work.

In our model the exterior tumour boundary is defined to be where the tumour cell volume fraction drops to zero. Thus we make the assumption that is common in models of this type of a sharp interface between the tumour and its surroundings (Ward and King 1999, Landman and Please 2001, Breward *et al* 2002, Byrne *et al* 2003). Some authors have developed models which relax this assumption and allow for a coexistence of tumour

and healthy cells (Hubbard and Byrne 2013). Such model extensions that explicitly include a normal cell phase may be useful in further investigations into tumour response dynamics and the impact of radiotherapy on the surrounding normal tissue.

By performing a parameter sweep on the sub-space describing the material properties of dead cellular material we examined the effects of some aspects of inter-patient heterogeneity on radiotherapy response. These may include differences in the balance of different cell death pathways induced by irradiation of the tumour cells (Eriksson and Stigbrand 2010), the strength of the immune response due to infiltration of immune cells and the subsequent clearance of dead material (Kaur and Asea 2012), interpatient heterogeneity in radiation sensitivity (Eschrich *et al* 2009), and simply biological variation (Spencer *et al* 2009). Model simulations suggest that the influence of the dead material is dependent on the wider region of parameter space. For some parameter combinations, tumour composition and growth trajectories may be very similar before radiotherapy but treatment response dynamics vary greatly. These results suggest that the material properties of the dead phase are significant, and further work would need to identify how early during the treatment we may reasonably determine tumour composition and tumour properties to reliably predict response in individual patients.

Acknowledgments

This work was funded in part by the Engineering and Physical Sciences Research Council (Grant No. EP/G037280/1). TL would also like to thank the Moffitt Cancer Center, where some of this work was undertaken, for their hospitality.

ORCID iDs

Thomas D Lewin https://orcid.org/0000-0002-6528-8936
Eduardo G Moros https://orcid.org/0000-0003-1964-2460

References

Ahmed K A, Correa C R, Dilling T J, Rao N G, Shridhar R, Trotti A M, Wilder R B and Caudell J J 2014 Altered fractionation schedules in radiation treatment: a review *Semin. Oncol.* **41** 730–50

Alfonso J C L, Jagiella N, Nunez L, Herrero M A and Drasdo D 2014 Estimating dose painting effects in radiotherapy: a mathematical model *PloS One* **9** e89380

Alper T and Howard-Flanders P 1956 Role of oxygen in modifying the radiosensitivity of *E. Coli* B *Nature* **178** 978–9

Bagher-Ebadian H, Siddiqui F, Liu C, Movsas B and Chetty I J 2017 On the impact of smoothing and noise on robustness of CT and CBCT radiomics features for patients with head and neck cancers *Med. Phys.* **44** 1755–70

Bertout J A, Patel S A and Simon M C 2008 The impact of O_2 availability on human cancer *Nat. Rev. Cancer* **8** 967–75

Bobadilla A V P, Maini P K and Byrne H 2018 A stochastic model for tumour control probability that accounts for repair from sublethal damage *Math. Med. Biol.* **35** 181–202

Boemo M A and Byrne H M 2019 Mathematical modelling of a hypoxia-regulated oncolytic virus delivered by tumour-associated macrophages *J. Theor. Biol.* **461** 102–16

Breward C J, Byrne H M and Lewis C E 2002 The role of cell-cell interactions in a two-phase model for avascular tumour growth *J. Math. Biol.* **45** 125–52

Byrne H M, King J R, McElwain D L S and Preziosi L 2003 A two-phase model of solid tumour growth *Appl. Math. Lett.* **16** 567–73

Carlson D J, Keall P J, Loo B W, Chen Z J and Brown J M 2011 Hypofractionation results in reduced tumor cell kill compared to conventional fractionation for tumors with regions of hypoxia *Int. J. Radiat. Oncol. Biol. Phys.* **79** 1188–95

Carlson D J, Stewart R D and Semenenko V A 2006 Effects of oxygen on intrinsic radiation sensitivity: a test of the relationship between aerobic and hypoxic linear-quadratic (LQ) model parameters *Med. Phys.* **33** 3105–15

Carmeliet P and Jain R K 2000 Angiogenesis in cancer and other diseases *Nature* **407** 249–57

Caudell J J, Torres-Roca J F, Gillies R J, Enderling H, Kim S, Rishi A, Moros E G and Harrison L B 2017 The future of personalised radiotherapy for head and neck cancer *Lancet Oncol.* **18** e266–73

Cheng B, Lin M, Huang G, Li Y, Ji B, Genin G M, Deshpande V S, Lu T J and Xu F 2017 Cellular mechanosensing of the biophysical microenvironment: a review of mathematical models of biophysical regulation of cell responses *Phys. Life Rev.* **22–3** 88–119

Chvetsov A V 2013 Tumor response parameters for head and neck cancer derived from tumor-volume variation during radiation therapy *Med. Phys.* **40** 034101

Chvetsov A V, Dong L, Palta J R and Amdur R J 2009 Tumor-volume simulation during radiotherapy for head-and-neck cancer using a four-level cell population model *Int. J. Radiat. Oncol. Biol. Phys.* **75** 595–602

Chvetsov A V, Rajendran J G, Zeng J, Patel S A, Bowen S R and Kim E Y 2017 Theoretical effectiveness of cell survival in fractionated radiotherapy with hypoxia-targeted dose escalation *Med. Phys.* **44** 1–8

Chvetsov A V, Yartsev S, Schwartz J L and Mayr N 2014 Assessment of interpatient heterogeneity in tumor radiosensitivity for nonsmall cell lung cancer using tumor-volume variation data *Med. Phys.* **41** 064101

Enderling H, Park D, Hlatky L and Hahnfeldt P 2009 The importance of spatial distribution of stemness and proliferation state in determining tumor radioresponse *Math. Model. Nat. Phenom.* **3** 117–33

Endlich B, Radford I R, Forrester H B and Dewey W C 2000 Computerized video time-lapse microscopy studies of ionizing radiation-induced rapid-interphase and mitosis-related apoptosis in lymphoid cells *Radiat. Res.* **153** 36–48

Ergun A, Camphausen K and Wein L M 2003 Optimal scheduling of radiotherapy and angiogenic inhibitors *Bull. Math. Biol.* **65** 407–24

Eriksson D and Stigbrand T 2010 Radiation-induced cell death mechanisms *Tumor Biol.* **31** 363–72
Eschrich S A *et al* 2009 A gene expression model of intrinsic tumor radiosensitivity: prediction of response and prognosis after chemoradiation *Int. J. Radiat. Oncol. Biol. Phys.* **75** 489–96
Fowler J F 2006 Development of radiobiology for oncology—a personal view *Phys. Med. Biol.* **51** R263–86
Gong J, Dos Santos M M, Finlay C and Hillen T 2013 Are more complicated tumour control probability models better? *Math. Med. Biol.* **30** 1–19
Grogan J A, Markelc B, Connor A J, Muschel R J, Pitt-Francis J M, Maini P K and Byrne H M 2016 Predicting the influence of microvascular structure on tumour response to radiotherapy *IEEE Trans. Biomed. Eng.* **3** 504–11
Hanahan D and Weinberg R A 2000 The hallmarks of cancer *Cell* **100** 57–70
Hanin L G 2004 A stochastic model of tumor response to fractionated radiation: limit theorems and rate of convergence *Math. Biosci.* **191** 1–17
Horsman M R, Wouters B G, Joiner M C and Overgaard J 2009 The oxygen effect, fractionated radiotherapy *Basic Clinical Radiobiology* ed M C Joiner and A J van der Kogel (Boca Raton, FL: CRC Press)
Hubbard M E and Byrne H M 2013 Multiphase modelling of vascular tumour growth in two spatial dimensions *J. Theor. Biol.* **316** 70–89
Joiner M and van der Kogel A 2009 *Basic Clinical Radiobiology Fourth Edition* (Boca Raton, FL: CRC Press)
Joiner M C 2009 Quantifying cell kill, cell survival ed M C Joiner and A J van der Kogel *Basic Clinical Radiobiology* (Boca Raton, FL: CRC Press)
Joiner M C, van der Kogel A J and Steel G G 2009 Introduction: the significance of radiobiology, radiotherapy for cancer treatment *Basic Clinical Radiobiology* ed M C Joiner and A J van der Kogel (Boca Raton, FL: CRC Press)
Kaur P and Asea A 2012 Radiation-induced effects and the immune system in cancer *Frontiers Oncol.* **2** 1–10
Landman K A and Please C P 2001 Tumour dynamics and necrosis: surface tension and stability *IMA J. Math. Appl. Med. Biol.* **18** 131–58
Ledzewicz U and Schättler H 2012 Multi-input optimal control problems for combined tumor anti-angiogenic and radiotherapy treatments *J. Optim. Theory Appl.* **153** 195–224
Lewin T D, Maini P K, Moros E G, Enderling H and Byrne H M 2018 The evolution of tumour composition during fractionated radiotherapy: implications for outcome *Bull. Math. Biol.* **80** 1207–35
Lewin T D, Maini P K, Moros E G, Enderling H and Byrne H M 2019 A three phase model to investigate the effects of dead material on the growth of avascular tumours *Math. Modelling Nat. Phenom.* (submitted)
Lewin T *et al* 2016 Proliferation saturation index predicts oropharyngeal squamous cell cancer gross tumor volume reduction to prospectively identify patients for adaptive radiation therapy *Int. J. Radiat. Oncol. Biol. Phys.* **94** 903
McAneney H and O'Rourke S F C 2007 Investigation of various growth mechanisms of solid tumour growth within the linear-quadratic model for radiotherapy *Phys. Med. Biol.* **52** 1039–54
O'Rourke S F C, McAneney H and Hillen T 2009 Linear quadratic and tumour control probability modelling in external beam radiotherapy *J. Math. Biol.* **58** 799–817
Poleszczuk J, Walker R, Moros E G, Latifi K, Caudell J J and Enderling H 2018 Predicting patient-specific radiotherapy protocols based on mathematical model choice for proliferation saturation index *Bull. Math. Biol.* **80** 1195–206
Powathil G G, Adamson D J and Chaplain M A 2013 Towards predicting the response of a solid tumour to chemotherapy and radiotherapy treatments: clinical insights from a computational model *PLoS Comput. Biol.* **9** e1003120
Powathil G G, Munro A J, Chaplain M A and Swat M 2016 Bystander effects and their implications for clinical radiation therapy: insights from multiscale in silico experiments *J. Theor. Biol.* **401** 1–14
Prokopiou S, Moros E G, Poleszczuk J, Caudell J, Torres-Roca J F, Latifi K, Lee J K, Myerson R, Harrison L B and Enderling H 2015 A proliferation saturation index to predict radiation response and personalize radiotherapy fractionation *Radiat. Oncol.* **10** 159
Richard M, Kirkby K J, Webb R P and Kirkby N F 2007 A mathematical model of response of cells to radiation *Nucl. Instrum. Methods Phys. Res.* B **255** 18–22
Rockne R, Alvord E C, Rockhill J K and Swanson K R 2009 A mathematical model for brain tumor response to radiation therapy *J. Math. Biol.* **58** 561–78
Rockne R C *et al* 2019 The 2019 mathematical oncology roadmap *Phys. Biol.* **16** 041005
Rockne R C *et al* 2015 A patient-specific computational model of hypoxia-modulated radiation resistance in glioblastoma using (18) F-FMISO-PET *J. R. Soc. Interface* **12** 20141174
Rockne R, Rockhill J K, Mrugala M, Spence A M, Kalet I, Hendrickson K, Lai A, Cloughesy T, Alvord E C and Swanson K R 2010 Predicting the efficacy of radiotherapy in individual glioblastoma patients *in vivo*: a mathematical modeling approach *Phys. Med. Biol.* **55** 3271–85
Sachs R K, Hlatky L R and Hahnfeldt P 2001 Simple ODE models of tumor growth and anti-angiogenic or radiation treatment *Math. Comput. Modelling* **33** 1297–305
Salem A *et al* 2019 Oxygen-enhanced MRI is feasible, repeatable, and detects radiotherapy-induced change in hypoxia in xenograft models and in patients with non-small cell lung cancer *Clin. Cancer Res.* **25** 3818–30
Scott J G, Fletcher A G, Anderson A R A and Maini P K 2016 Spatial metrics of tumour vascular organisation predict radiation efficacy in a computational model *PLoS Comput. Biol.* **1** 1–24
Sharma S, Bekelman J, Lin A, Lukens J N, Roman B R, Mitra N and Swisher-McClure S 2016 Clinical impact of prolonged diagnosis to treatment interval (DTI) among patients with oropharyngeal squamous cell carcinoma *Oral Oncol.* **56** 17–24
Spencer S, Gaudet S, Albeck J, Burke J and Sorger P 2009 Non-genetic origins of cell-to-cell variability in TRAIL-induced apoptosis *Nature* **7245** 428–32
Stevens C, Bondy S J and Loblaw D A 2010 Wait times in prostate cancer diagnosis and radiation treatment *Can. Urological Assoc. J.* **4** 243–8
Sun Y, Reynolds H M, Wraith D, Williams S, Finnegan M E, Mitchell C, Murphy D and Haworth A 2018 Voxel-wise prostate cell density prediction using multiparametric magnetic resonance imaging and machine learning *Acta Oncol.* **57** 1540–6
Tariq I, Chen T, Kirkby N F and Jena R 2016 Modelling and Bayesian adaptive prediction of individual patients' tumour volume change during radiotherapy *Phys. Med. Biol.* **61** 2145–61
Wang L, Correa C R, Hayman J A, Zhao L, Cease K, Brenner D, Arenberg D, Curtis J, Kalemkerian G P and Kong F M 2009 Time to treatment in patients with stage III non-small cell lung cancer *Int. J. Radiat. Oncol. Biol. Phys.* **74** 790–5
Wang P and Feng Y 2013 A mathematical model of tumor volume changes during radiotherapy *Sci. World J.* **2013** 181070
Ward J P and King J R 1999 Mathematical modelling of avascular-tumour growth. II: Modelling growth saturation *IMA J. Math. Appl. Med. Biol.* **16** 171–211
Wheldon T E, Kirk J and Orr J S 1977 Optimal radiotherapy of tumour cells following exponential-quadratic survival curves and exponential repopulation kinetics *Br. J. Radiol.* **50** 681–2
Zaider M and Hanin L 2011 Tumor control probability in radiation treatment *Med. Phys.* **38** 574–83
Zaider M and Minerbo G N 2000 Tumour control probability: a formulation applicable to any temporal protocol of dose delivery *Phys. Med. Biol.* **45** 279–93